ADVANCES IN ATMOSPHERIC SCIENCES, VOL. 38, OCTOBER 2021, 1737–1749

• **Original Paper** •

The Role of Ocean Dynamics in the Cross-equatorial Energy Transport under a Thermal Forcing in the Southern Ocean

Fukai LIU*[1,2,3], Yiyong LUO[1,2,3], Jian LU[4], and Xiuquan WAN[1,2,3]

[1]*Frontier Science Center for Deep Ocean Multispheres and Earth System (FDOMES) and Physical Oceanography Laboratory*, *Ocean University of China*, *Qingdao* 266100, *China*

[2]*Laboratory for Ocean Dynamics and Climate*, *Qingdao Pilot National Laboratory for Marine Science and Technology*, *Qingdao* 266100, *China*

[3]*College of Oceanic and Atmospheric Sciences*, *Ocean University of China*, *Qingdao* 266100, *China*

[4]*Atmospheric Sciences and Global Change Division*, *Pacific Northwest National Laboratory*, *Richland*, *WA* 99352, *USA*

(Received 3 March 2021; revised 6 May 2021; accepted 19 May 2021)

ABSTRACT

Under external heating forcing in the Southern Ocean, climate models project anomalous northward atmosphere heat transport (AHT) across the equator, accompanied by a southward shift of the intertropical convergence zone (ITCZ). Comparison between a fully coupled and a slab ocean model shows that the inclusion of active ocean dynamics tends to partition the cross-equatorial energy transport and significantly reduce the ITCZ shift response by a factor of 10, a finding which supports previous studies. To understand how ocean dynamics damps the ITCZ's response to an imposed thermal heating in the Southern Ocean, we examine the ocean heat transport (OHT) and ocean circulation responses in a set of fully coupled experiments. Results show that both the Indo-Pacific and the Atlantic contribute to transport energy across the equator mainly through its Eulerian-mean component. However, different from previous studies that linked the changes in OHT to the changes in the wind-driven subtropical cells or the Atlantic meridional overturning circulation (AMOC), our results show that the cross-equatorial OHT anomaly is due to a broad clockwise overturning circulation anomaly below the subtropical cells (approximately bounded by the 5°C to 20°C isotherms and 50°S to 10°N). Further elimination of the wind-driven component, conducted by prescribing the climatological wind stress in the Southern Ocean heat perturbation experiments, leads to little change in OHT, suggesting that the OHT response is predominantly thermohaline-driven by air-sea thermal interactions.

Key words: Southern Ocean, ocean dynamics, atmospheric energy transport, oceanic energy transport

Citation: Liu, F. K., Y. Y. Luo, J. Lu, and X. Q. Wan, 2021: The role of ocean dynamics in the cross-equatorial energy transport under a thermal forcing in the Southern Ocean. *Adv. Atmos. Sci.*, **38**(10), 1737–1749, https://doi.org/10.1007/s00376-021-1099-6.

Article Highlights:

- Under external forcing in the Southern Ocean, the ocean dynamics alleviate the burden of the atmosphere in cross-equatorial energy transport.
- Both the Indo-Pacific and the Atlantic act to transport anomalous energy northward via changing its circulation.
- The above change in circulation is predominately driven by thermohaline dynamics rather than by wind stress.

1. Introduction

Using thermodynamic slab ocean models, previous studies (e.g., Chiang and Bitz, 2005; Broccoli et al., 2006; Kang et al., 2008; Hwang and Frierson, 2013; Hwang et al., 2017) have found a great impact of hemispherically asymmetric forcing on global climate, especially on the zonal mean position of the intertropical convergence zone (ITCZ). For example, heating in the Southern Ocean can warm the atmosphere of the southern hemisphere and cause a northward, cross-equatorial atmosphere heat transport (AHT) anomaly, which induces a southward moisture flux anomaly and thus shifts the ITCZ southward. However, in a fully coupled model with active ocean dynamics, the hemispheric-scale energy imbalance can be restored by the atmosphere and the ocean together, and the ocean is the more efficient of the

* Corresponding author: Fukai LIU
Email: fliu@ouc.edu.cn

two in transporting energy in the tropics. This is because the strongly stratified ocean can efficiently transport energy away from the equator, whereas the atmosphere is less efficient at transporting energy in the tropics due to the weak moist static energy gradient associated with the moist convection and the weak effects of rotation (Klinger and Marotzke, 2000; Held, 2001; Czaja and Marshall, 2006). Therefore, ocean dynamics can lead to the partitioning of cross-equatorial energy transport such that the response in cross-equatorial AHT and the ITCZ shift is largely damped (Kay et al., 2016; Hawcroft et al., 2017; Green and Marshall, 2017; Yu and Pritchard, 2019).

Still, through what mechanisms the ocean dynamics buffers the ITCZ shift remains an issue of debate, especially concerning the relative importance of the wind-driven and the thermohaline dynamical processes. Recently, Green and Marshall (2017) coupled the atmosphere with a dynamic ocean in a highly idealized two-basin model and perturbed the system with a hemispherically asymmetric forcing (that is, heating in the southern hemisphere but cooling in the northern hemisphere). Compared to the motionless slab ocean model, they found the ITCZ shift in the coupled model to be considerably damped by a factor of 4. This damped ITCZ shift response has been ascribed to the coupling between the Hadley cell and the ocean's wind-driven subtropical cell. Specifically, in response to the southern hemisphere heating and northern hemisphere cooling, the easterly trade winds show a weakening in the southern tropics and strengthening in the northern tropics, both wind anomalies act to induce an anomalous northward Ekman flow in the upper ocean. This cross-equatorial flow transports warm water and energy northward, strongly reducing the burden of the AHT and offsetting the imposed energy contrast between hemispheres, thus buffering the shift of ITCZ. In addition, this important role of wind-driven circulation in muting ITCZ shift has been discussed in other modeling studies (e.g., Held, 2001; Schneider et al., 2014; Kay et al., 2016).

Some other studies suggested that changes in Atlantic meridional overturning circulation (AMOC) can also contribute to damping the ITCZ shift (Frierson et al., 2013; Fučkar et al., 2013; Marshall et al., 2014; He et al., 2019; Yu and Pritchard, 2019), because the AMOC can transport an energy anomaly across the equator, reducing the hemispherical energy imbalance and thereby muting the ITCZ shift. In particular, a recent work of Yu and Pritchard (2019) performed similar experiments as Green and Marshall (2017) but with a more realistic fully coupled model. Through placing hemispherically asymmetric perturbations in different latitudes, they found increasing importance of the AMOC responses in muting the ITCZ shift, and the AMOC becomes equally important as the wind-driven subtropical cells when the forcing is placed at high latitudes.

The above studies highlighted the important role of ocean dynamics in partitioning cross-equatorial energy transport and in modulating the ITCZ shift, but much work remains to be done to understand the physical mechanisms. Here, we employ the slab ocean and fully coupled version of the Community Earth System Model 1 (CESM1) to systematically compare the climate response to a pair of heating and cooling forcings placed upon the Southern Ocean. The reason we place the forcing in the Southern Ocean is due to its large climatic influence (Hwang et al., 2017; Liu et al., 2018b), and to facilitate the comparison with many previous studies that placed external forcing in similar regions (Kay et al., 2016; Hawcroft et al., 2017; Hwang et al., 2017; Yu and Pritchard, 2019). To understand how ocean dynamics modulate the cross-equatorial energy transport, we further perform a set of partially coupled experiments in which the wind stress is prescribed to a repeating climatology, and thereby the wind-driven oceanic circulation responses can be isolated. As to be shown later, the ocean can transport a similar amount of energy across the equator even after the wind-driven ocean dynamical adjustment is disabled, and the response in ocean heat transport (OHT) is predominantly thermohaline-driven by air-sea thermal interactions.

The remainder of the paper is structured as follows. Section 2 describes the slab ocean and the fully coupled model, the design of experiments, and metrics used in this study. Section 3 compares the climate response in the slab ocean and fully coupled experiments. Section 4 illustrates how ocean dynamics modulates the cross-equatorial energy transport. Section 5 summarizes the main conclusions of the study and provides a brief discussion.

2. Methods

2.1. *Coupled and partially coupled experiments*

The model we use includes both the fully coupled and the slab ocean version of the Community Earth System Model version 1 (CESM1). The fully coupled model (CESM1-CPL) is comprised of the Community Atmosphere Model version 5, the Community Land Model version 4, the Community Ice CodE, and the Parallel Ocean Program version 2. For both atmosphere and land models, the horizontal resolution is 2.5° longitude × 1.9° latitude, with the atmospheric component discretized on 30 uneven vertical levels. For the sea ice model and ocean models, the horizontal resolution is at a nominal 1°, telescoped meridionally to ~0.3° at the equator. Vertically, the ocean model has 60 uneven levels with the thickness varying from 10 m near the surface to 250 m at the bottom. It should be noted that we run all the following experiments with perpetual equinox conditions, which reduces complexities in the results.

Starting from an equilibrium state that is available at NCAR, a control simulation (CTRL-CPL; Table 1) is integrated for 120 years under equinoctial solar radiation. We then perform two experiments with additional heating and cooling band forcing Q^* added to the Southern Ocean, and they are denoted as HEAT-CPL and COOL-CPL. In such a way the total surface heat flux Q_t into the Southern Ocean can be expressed as $Q_t = Q_{ao} + Q^*$, where Q_{ao} is the sum of radiative and turbulent heat fluxes. Q^* is designed to be a 24°-wide band with the maximum amplitude of +/−12

Table 1. Experiments with fully coupled and slab ocean CESM1.

NAME	RUN (yrs)	DESCRIPTION
		Fully coupled experiments
CTRL-CPL	120	Fully coupled control run
HEAT-CPL	120	Perturbed by an additional heating in the Southern Ocean
COOL-CPL	70	Perturbed by an additional cooling in the Southern Ocean
		Wind stress overriding experiments
HEAT-WS	70	Same as HEAT-CPL, but wind stress is specified to climatology
COOL-WS	70	Same as COOL-CPL, but wind stress is specified to climatology
		Slab ocean experiments
CTRL-SOM	100	Slab ocean control run
HEAT-SOM	80	Perturbed by an additional heating in the Southern Ocean
COOL-SOM	80	Perturbed by an additional cooling in the Southern Ocean

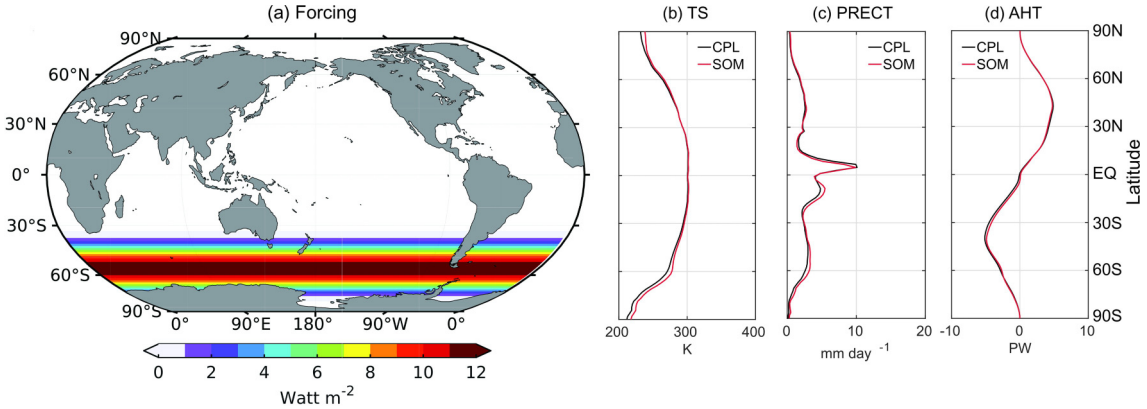

Fig. 1. (a) Geographical locations of the energy perturbation bands. The zonal mean climatology of (b) TS (K), (c) precipitation (mm d^{-1}), and (d) AHT (PW) in CTRL-CPL (black) and CTRL-SOM (red). TS = surface temperature; AHT = atmospheric heat transport.

W m^{-2} at 55°S (Fig. 1a), and the area mean heat flux perturbation over the forced ocean is +/− 4.8 W m^{-2}. Each simulation is integrated for 70 years, and the data of the last 40 years are used for estimating the forced response by subtracting the CTRL-CPL data therefrom. To check how symmetric the climate response is to the heating and cooling thermal forcings in the Southern Ocean, we estimate the symmetric and asymmetric response as $X_1 = (\delta X_+ - \delta X_-)/2$ and $X_n = (\delta X^+ + \delta X^-)/2$, respectively. Admittedly, the climate system in our work is still far from equilibrium because of the sluggish deep ocean (Long et al., 2014; Stouffer, 2004), and the precise depiction of the atmospheric and oceanic responses at their full equilibrium stage is beyond the scope of this study. A recent study by Lembo et al. (2020) examined the response of global ocean heat uptake to an abrupt doubling of CO_2 and found that the anomaly of global ocean heat uptake displays two prominent time scales: the fast response in which the upper ocean is in quasi-equilibrium with the radiative forcing, and the subsequent slow response owing to the gradual adjustment of the deep ocean. The timescale of the fast ocean heat uptake response is on the order of a few decades, while the timescale of the slow response is thousands of years or longer, which is too computationally expensive with the fully coupled model. However, as shown later, most of the oceanic temperature, density and circulation changes in this study occur in the upper ocean (< 800 m), the timescales for these fast responses are relatively short and can be separated from the millennial timescale for deep ocean equilibration. In addition, we extend the HEAT-CPL run to 120 years, and the precipitation, TS, zonal mean temperature, and MOC anomalies averaged over years 70 to 120 are indeed very similar to those over years 30 to 70 (Fig. 2), giving confidence that the responses discussed in this study are steady and robust.

To disable the wind-driven oceanic processes, we further perform a pair of partially coupled heating and cooling experiments (HEAT-WS and COOL-WS; Table 1). The partial coupling is realized through overriding the wind stress at the air-sea interface to a daily mean climatology (also see Liu et al., 2017a for details), which is derived from the 120-year CTRL-CPL run. Therefore, the OHT, as well as ocean circulation changes, are a result of air-sea thermal interaction, and the wind stress contribution to the oceanic changes can be estimated by subtracting the results of CPL-WS from those in CPL. This technique has been successfully used to examine the formation processes of SST in response to global warming in many previous studies (Lu and Zhao,

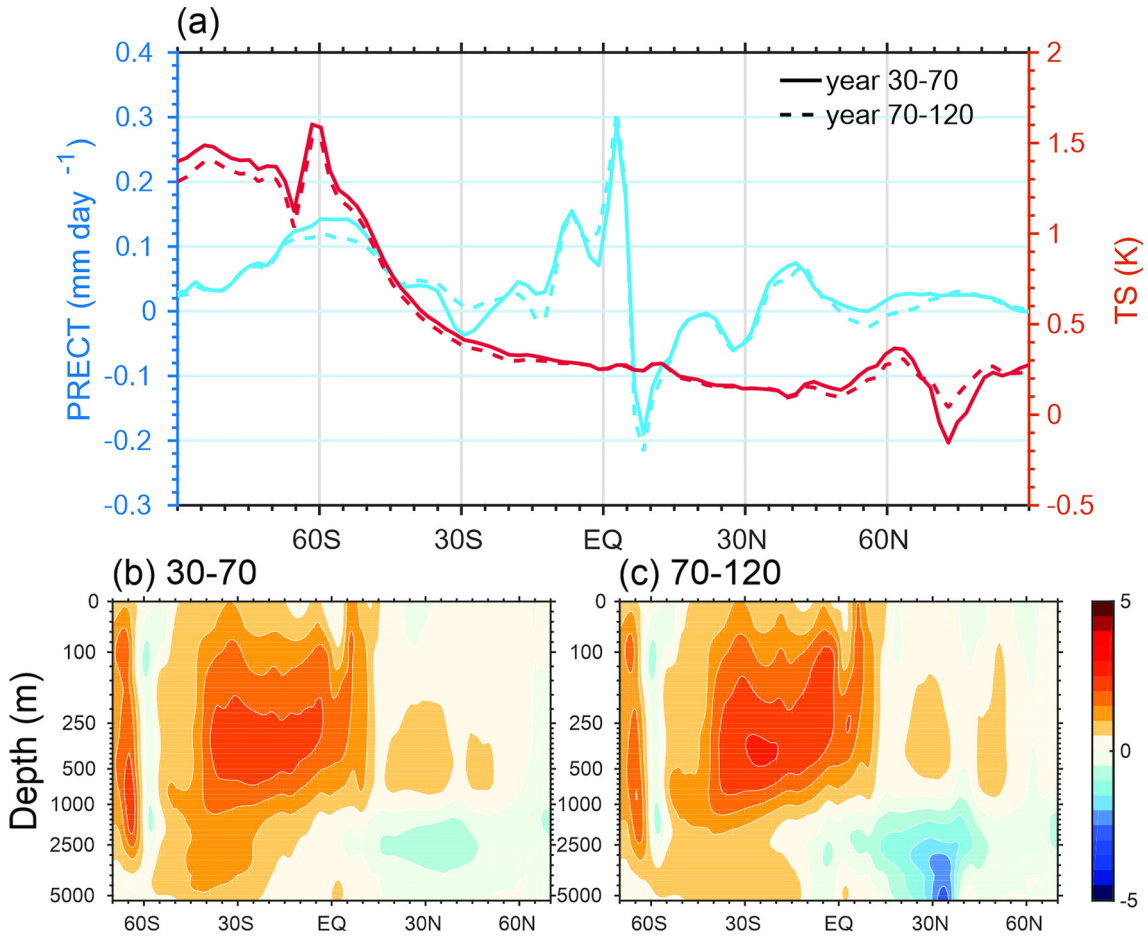

Fig. 2. (a) Zonal mean precipitation (blue lines; left axis) and TS (red lines; right axis) responses in CPL-HEAT averaged over years 30 to 70 (solid lines) and years 70 to 120 (dashed lines). (b–c) The total MOC response (Sv) in CPL-HEAT averaged over years 30 to 70 and years 70 to 120.

2012; Luo et al., 2015; Liu et al., 2017a, b).

2.2. *Slab ocean experiments*

To test the impact of the active ocean dynamics, we also use a slab ocean version of CESM1 (CESM1-SOM). In this model, the ocean and atmosphere are only thermodynamically coupled, and SST is computed from surface heat flux and q-flux that accounts for the missing ocean dynamics. We integrate a slab ocean control run (CTRL-SOM) for 100 years, both the mixed layer depth and the q-flux are derived from the climatology of CTRL-CPL. The q-flux is allowed to vary in space and has a repeating seasonal cycle, while the mixed layer depth is only allowed to vary in space. Branching out from the 21st year of the control run, a pair of heating and cooling experiments are integrated for 80 years with the same band forcing Q^* added to or subtracted from the Southern Ocean (HEAT-SOM and COOL-SOM; Table 1). Again, only the last 40 years of the model integration are used for analysis.

The zonal mean climatology of surface temperature (TS), precipitation, and AHT in the coupled and the slab models are compared in Figs. 1b–d. Although some minor differences can be found between them, the large-scale distributions are remarkably similar, legitimizing the following comparison of their responses to the same external forcing.

2.3. *Oceanic heat transport*

Following Yang et al. (2015), the zonally integrated full-depth OHT ($\mathrm{OHT_{Tot}}$) can be calculated as the residual of three components:

$$\begin{aligned}\mathrm{OHT_{Tot}} &= \rho_0 c_p \iint_{-H}^{0} (\bar{v}\theta + v^*\theta + D)\,\mathrm{d}z\mathrm{d}x \\ &= \mathrm{OHT_{Eul}} + \mathrm{OHT_{Ed}} + \mathrm{OHT_{Diff}}\,, \end{aligned} \quad (1)$$

where ρ_0 is the density of seawater, c_p is the specific heat of seawater, θ is potential temperature, $\bar{v}$ and v^* are Eulerian-mean and eddy-induced meridional velocity, respectively, D denotes diffusion and other subgrid processes. Therefore, the total OHT is decomposed into components induced by Eulerian-mean flow, eddies, and diffusion. Among the three components, the Eulerian-mean component can be easily calculated with model output potential temperature and Eulerian-mean velocity. The eddy component, which results from both mesoscale and sub-mesoscale processes, is not resolved in our ocean model. Instead, the mesoscale

eddies are parameterized by the Gent–McWilliams scheme (Gent and McWilliams, 1990), in which a variable coefficient enables an appropriate ocean response to surface momentum forcing. The sub-mesoscale eddies are parameterized following Fox-Kemper et al. (2008).

The response of the Eulerian-mean OHT can be further decomposed into the advection of mean temperature by the circulation anomaly, the advection of temperature anomaly by mean circulation, and a nonlinear component, i.e.,

$$\rho_0 c_p \iint_{-H}^{0} \Delta(\overline{v}\overline{\theta})\,\mathrm{d}z\mathrm{d}x = \rho_0 c_p \iint_{-H}^{0} (\overline{\theta}\Delta\overline{v} + \overline{v}\Delta\overline{\theta} + \Delta\overline{v}\Delta\overline{\theta})\,\mathrm{d}z\mathrm{d}x\,. \tag{2}$$

Following Yu and Pritchard (2019), we term them as dynamic, thermodynamic, and nonlinear components, respectively.

On the other hand, the total OHT can be separated into contributions from individual basins. Since the mass flow in the Indian Ocean or the Pacific Ocean alone is not closed due to the Indonesian Throughflow, the heat transport of the two basins is summed together.

2.4. *Meridional Overturning Circulation*

The MOC is calculated by integrating meridional velocity zonally and vertically. Since the meridional velocity can be decomposed into Eulerian-mean and eddy-induced components $v = \overline{v} + v^*$, the MOC can also be decomposed into these two components:

$$\begin{aligned}\psi_{\mathrm{Tot}} &= \iint_{-H}^{0} (\overline{v} + v^*)\mathrm{d}z\mathrm{d}x \\ &= \psi_{\mathrm{Eul}} + \psi_{\mathrm{Ed}}\,.\end{aligned} \tag{3}$$

3. Climate response in fully coupled and slab ocean models

Figure 3 presents an overall survey of the annual mean TS, precipitation, zonal wind stress, and sea ice area response in both the CLP and SOM experiments. First, through the examination of the zonal mean responses in the right-hand panels, we find the climate response to heating and cooling perturbations is remarkably symmetric in both CPL and SOM, that is, the asymmetric response (dashed lines in the right panels) is an order of magnitude smaller than the corresponding symmetric response. Therefore, we will focus on the symmetric response in the following discussion.

A heating perturbation in the Southern Ocean will inject energy into the surface ocean and warm both the ocean and the overlying atmosphere, consequently, the TS response in the Southern Ocean is characterized by a circumpolar belt of enhanced warming. Some of the warmth spreads to the northern hemisphere, especially over the monsoonal regions (Figs. 3a, b). As the ITCZ tends to shift towards the warmed hemisphere, there is a clear meridional dipole in the precipitation response, indicative of a southward shift (Figs. 3c, d). The pattern of zonal wind stress anomalies shows a weakening of the trade winds in the southern hemisphere and a strengthening in the northern hemisphere, which is consistent with a southward shift of the ITCZ (Figs. 3c, f). These results agree well with Hwang et al (2017), who examined the global response to a change in the Southern Ocean heat uptake within a slab ocean model. There is a notable spatial similarity in the precipitation response between the SOM and CPL experiments (pattern correlation = 0.63), indicative of the energetic constraint on the ITCZ response. The similarity is also present in the response of zonal wind stress, despite the active ocean dynamical feedback in the CPL case. In response to the surface warming in the Southern Ocean, the sea ice poleward of 55°S experiences a clear decrease in both models. In contrast, the sea ice melting in the northern hemisphere is much weaker, corresponding to the relatively small TS warming there. Note that the heat flux perturbation is specified as a meridionally-oriented cosine hump, the forcing magnitude decreases from 12 W m^{-2} at 55°S to zero at 67°S and the mean heat flux perturbation over the sea ice-covered ocean is about 5.5 W m^{-2}. Therefore, the sea ice response in the Southern Ocean is mild and its magnitude is comparable with that under the moderate RCP4.5 emissions scenario. Despite the above similarities between CPL and SOM, notable differences can still be found in their patterns. For example, the TS response in CPL is highly concentrated in the Southern Ocean and peaks near the ice edge, whereas the TS anomaly covers a broader region in the southern hemisphere and peaks over the Antarctic continent in the SOM experiments. In addition, the zonal wind anomalies are mainly confined to the Pacific basin in CPL, whereas they cover almost the whole tropical oceans in SOM (Figs. 3c, f), resulting in a larger hemispherical asymmetry in the tropics. Apart from the above pattern differences, the largest difference between the two models is the magnitude of the anomalies. All the responses become considerably smaller when active ocean dynamics are included, especially in the Southern Ocean and the tropics, largely due to the energy uptake by the active ocean. In CPL, the Southern Ocean releases a 1.2 W m^{-2} heat flux anomaly (areal mean over the forced region) into the atmosphere, which is only a quarter of that in SOM. Therefore, most of the energy imbalance is absorbed by the active ocean and works to change its thermal structure and circulation.

Figure 4 shows the response of AHT and the shift of ITCZ. The location of the ITCZ is measured as the latitudinal centroid of precipitation P

$$\phi_{\mathrm{ITCZ}} = \frac{\int_{\phi_1}^{\phi_2} \phi' \cos(\phi') P \mathrm{d}\phi'}{\int_{\phi_1}^{\phi_2} \cos(\phi') P \mathrm{d}'\phi}\,, \tag{4}$$

$$\phi_{\mathrm{ITCZ}} = \frac{\int_{\phi_1}^{\phi_2} \phi \cos(\phi) P \mathrm{d}\phi}{\int_{\phi_1}^{\phi_2} \cos(\phi) P P \mathrm{d}\phi}\,, \tag{5}$$

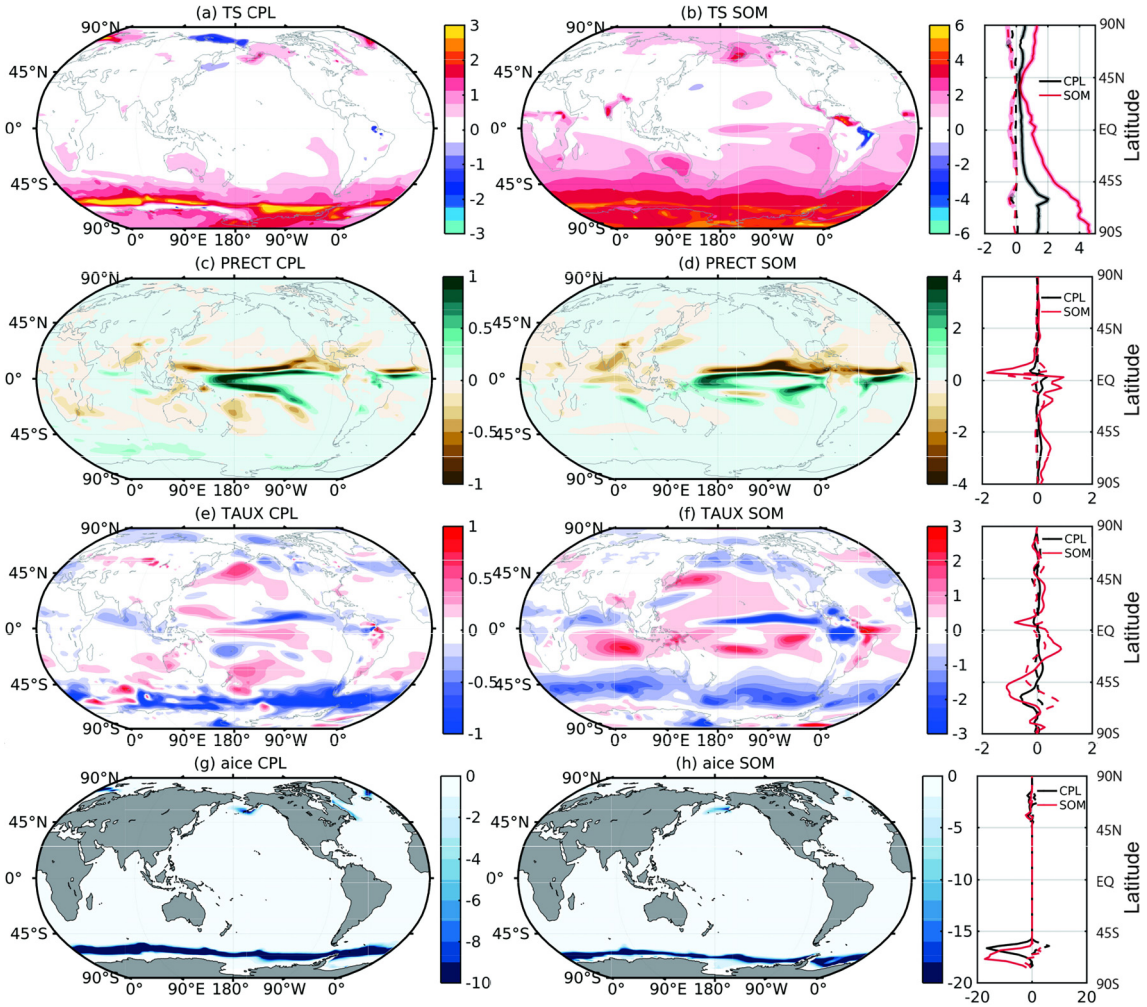

Fig. 3. Symmetric TS (°K), precipitation (mm d^{-1}), zonal wind stress, and sea ice area (%) responses (10^{-2} Nm^{-2}) in (left) CPL and (middle) SOM. Note different color bars in CPL and SOM. The right-hand panels show zonal mean symmetric (solid lines) and asymmetric (dashed lines) responses, with the latitude ranges at which the TS response is statistically significant at the 99% confidence level highlighted with shaded edges. The significance test is against the null hypothesis that a 20-year mean anomaly can randomly occur from internal variability, and the corresponding probability distribution is constructed from 5000 samples randomly picked from the control run of each experiment set.

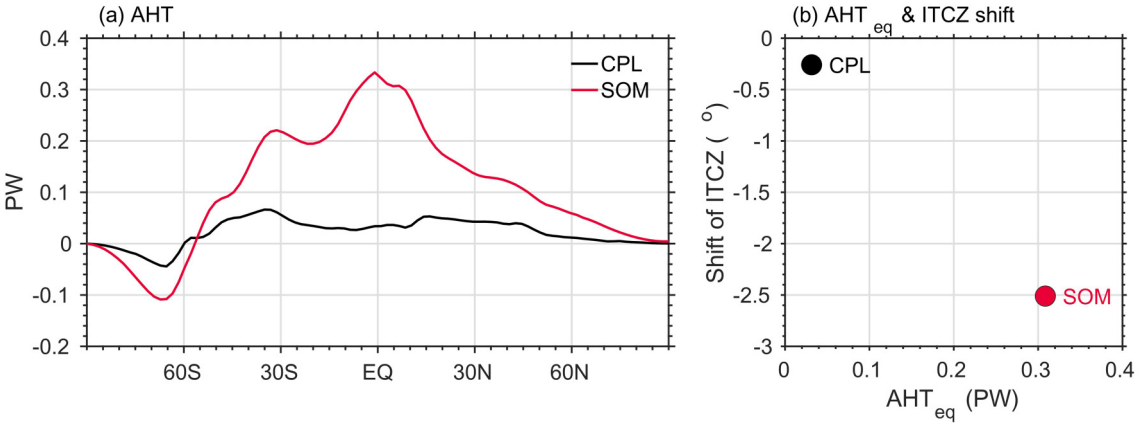

Fig. 4. (a) AHT response (PW) in CTRL-CPL (black) and CTRL-SOM (red). (b) The shift of ITCZ (*y*-axis) and the cross-equatorial AHT response in CTRL-CPL (black) and CTRL-SOM (red). The cross-equatorial AHT is calculated as the AHT average between 10°S–10°N. ITCZ = intertropical convergence zone.

where ϕ is the latitude and ϕ_1 = 20°S and ϕ_2 = 20°N are the latitude bounds for the integration. The cross-equatorial AHT is estimated as an average from 10°S–10°N. When additional energy is injected into the Southern Ocean, the atmosphere acts to transport the anomalous energy northward and across the equator in both CPL and SOM (Fig. 4a). However, the magnitude of AHT in CPL is considerably reduced in comparison to that in SOM, and their shapes differ substantially. The AHT anomaly in SOM shows a peak near the equator whereas that in CPL is slightly decreased near the equator. As a result, the inclusion of ocean dynamics acts to reduce the response in cross-equatorial AHT by 90% (from 3.1 PW to 0.3 PW; Fig. 4b). Since the shift of the ITCZ is controlled by the change in the cross-equatorial AHT (Donohoe et al., 2014; Frierson et al., 2013), the southward shift of the ITCZ is also reduced by an order of magnitude in CPL compared to SOM (from –2.5° to –0.25°; Fig. 4b).

4. OHT and MOC responses

The above comparison points to the importance of active ocean dynamics in modulating climate response, a natural follow-up inquiry concerns the mechanisms by which the ocean transports energy northward. To address this issue, we will explore the changes in OHT and MOC, with special attention given to the contribution from wind-driven ocean processes, consistent with the effect previously identified through comparing oceanic responses in CPL and CPL-WS experiments.

The mean OHT and MOC as well as their decomposition are shown in Fig. 5. Overall, the background mean OHT is featured with a hemispherically antisymmetric poleward heat transport, which is in good agreement with many previous studies (Held, 2001; Trenberth and Caron, 2001; Czaja and Marshall, 2006; Yang and Dai, 2015). As explained in Section 2.3, the total OHT can be decomposed into contributions from the Eulerian-mean circulation, the eddies, and diffusive processes. The total OHT is dominated by its Eulerian-mean component except in the Southern Ocean where eddies play a dominant role, as the poleward Eulerian-mean OHT observed there is largely suppressed due to the northward circumpolar Ekman flow. Therefore, the total southward OHT around 40°S is primarily maintained by the mesoscale and sub-mesoscale eddies (Jayne and Marotzke, 2002; Treguier et al., 2007; Yang and Dai, 2015). Figures 5d and 5f show the mean MOC in temperature-latitude coordinates. In this way, we can intuitively examine the heat transport due to different circulation features by comparing the temperature difference between the upper and lower branches (Held, 2001). Another advantage provided by this temperature coordinate plot is a clear separation of warm subtropical cells and cold deep cells. The warm cells are mostly wind-driven and span the temperature range from 10°C in the mid-latitudes to 28°C at the equator, whereas the cold cell is largely the thermohaline AMOC and spans the temperature between 2°C to 10°C. It is also evident that the eddy-induced transport acts to counter the Eulerian transport in the mid-to-high latitudes in the Southern Ocean (Fig. 5f). All of these features are in good agreement with previous studies (Farneti and Vallis, 2013; Yang et al., 2015, Dai et al., 2017).

When extra heat is injected into the Southern Ocean, a dynamically active ocean will transport energy northward,

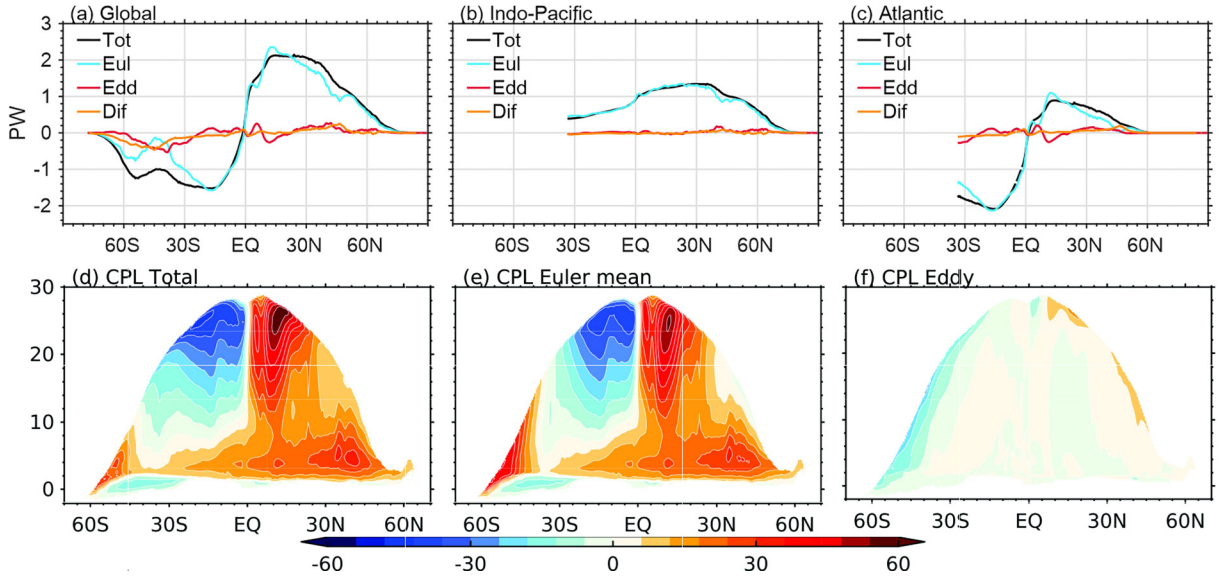

Fig. 5. (upper panel) The mean OHT (PW) for (a) the global oceans, (b) the Indo-Pacific Ocean, and (c) the Atlantic Ocean in CTRL-CPL. The total OHT (black) is decomposed into Eulerian-mean (blue), eddy (red), and diffusion (orange) components (lower panel). The mean MOC (Sv) in the temperature-latitude coordinate in CTRL-CPL. The total MOC is the residual of (d) the Eulerian-mean, (e) eddy, and (f) diffusion components, with positive (negative) values indicating a clockwise (counter-clockwise) circulation. OHT = ocean heat transport; MOC = meridional overturning circulation.

in the same direction as the atmosphere (Fig. 6). The anomalous cross-equatorial OHT largely reduces the burden of AHT compared to SOM (Fig. 4) and hence damps the shifting response of the ITCZ. A further decomposition shows that the change in the total OHT is dominated by its Eulerian-mean component (blue lines in Fig. 6). The eddy and diffusive components individually may not be negligible in the Southern Ocean, yet there is a large cancellation between the two components and their combination contributes negligibly to the total OHT response. Another important feature in the OHT response is that both the Indo-Pacific and Atlantic are important in transporting the anomalous energy northward (Figs. 6b, c). Of the total 0.18 PW cross-equatorial OHT response, the contribution from the Atlantic is 0.08 PW, slightly smaller in magnitude than that from the Indo-Pacific (0.10 PW). This result supports the recent finding of Yu and Pritchard (2019) that the Atlantic is an equally important contributor as the Indo-Pacific when the forcing is placed in high latitudes. On the other hand, due to a much smaller transport in the Pacific through the Bering Strait (Aagaard and Greisman 1975), the Atlantic dominates the anomalous OHT in the high latitudes of the northern hemisphere.

Since the Eulerian-mean component dominates the total OHT response, we then focus on its response and decompose it into the dynamic, thermodynamic, and nonlinear components (Eq. 2). The dynamic OHT response refers to the advection of the mean temperature by the circulation anomaly, while the thermodynamic response can be conceptualized as the advection of the temperature anomaly by the mean circulation. Figure 7a shows the cross-equatorial Eulerian-mean OHT and its breakdown in individual basins as well as its different components. Overall, the dynamic component has a much larger contribution to the global OHT response than the thermodynamic one, though differences exist in different basins. In the Indo-Pacific, the northward dynamic OHT response overwhelms the southward thermodynamic response, resulting in a net northward OHT anomaly. In contrast, the thermodynamic and dynamic components work in tandem to enhance the northward OHT in the Atlantic, although the magnitude of the former is somewhat smaller. The nonlinear response is not discussed here because of its negligible contribution.

In the Indo-Pacific, the ocean can transport large amounts of energy across the equator by changing its circulation (dynamic component), which appears to agree with the mechanism proposed by Green and Marshall (2017) that relates the change in cross-equatorial OHT to the change in wind stress in a highly idealized coupled model. Specifically, in response to the intensified (suppressed) easterly trades to the north (south) of the equator (Fig. 3e), the poleward Ekman flow in the upper ocean will be enhanced (weakened) to the north (south), leading to an anomalous northward Ekman flow across the equator. Since this anomalous northward flow stimulates a clockwise oceanic circulation centered at the equator and transports relatively warm (cold) water northward (southward) in the upper (lower) ocean, the atmosphere does not need to transport as much energy across the equator as in the SOM. Therefore, the oceanic circulation in the tropical Pacific is coupled to the atmospheric circulation through the zonal wind stress (e.g., Held, 2001; Green and Marshall, 2017; Schneider, 2017; Kang et al., 2018).

To examine the above mechanism highlighting the role of wind stress, we rerun the heating and cooling experiments, but with the wind-driven ocean circulation feedback disabled by prescribing the wind stress in every model step (CPL-WS experiments). The resultant OHT response and its decomposition are presented in Fig. 7b. As expected, due to the dominant role of the thermohaline circulation in driving the Atlantic OHT (Yang et al., 2015), shutting down the wind stress effect barely influences the total OHT in the Atlantic basin. However, it is intriguing that the Indo-Pacific is capable of transporting similar amounts of energy across the equator (Fig. 7b), with the wind-driven feedback effect accounting for only 1/6 of the 0.12 PW cross-equatorial OHT response. The wind-induced reduction in the cross-equatorial OHT is consistent in sign with what is proposed in Green and Marshall (2017), but its amplitude is much weaker. This result suggests that the circulation changes, as well as OHT changes in the Indo-Pacific, are largely thermohaline-driven rather than wind-driven.

To elaborate on the circulation-induced energy transport across the equator, we next show the changes in the MOC (Fig. 8) and zonal mean temperature (Fig. 9), which have been identified to be responsible for the dynamic and thermodynamic components of the OHT responses mentioned above. Note that only the Eulerian-mean MOC response is presented because of its dominant role in driving the total OHT (Fig. 6). As expected, the strengthened

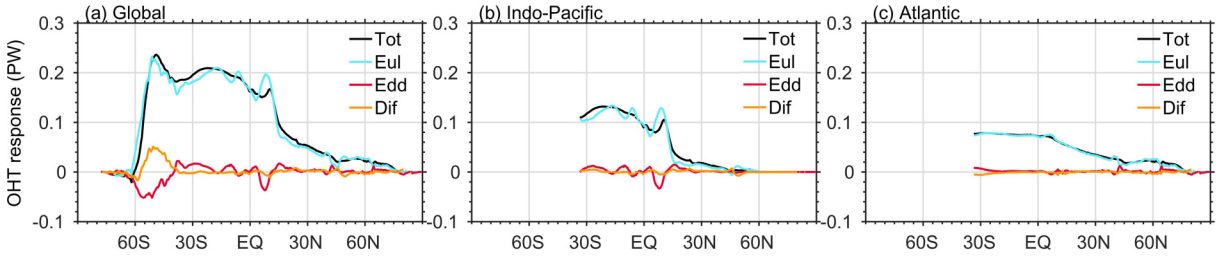

Fig. 6. The OHT response (PW) for (a) the global ocean, (b) the Indo-Pacific, and (c) the Atlantic. The total OHT is decomposed into Eulerian-mean (blue), eddy (red), and diffusion (orange) components.

(weakened) easterlies in the northern (southern) tropics lead to positive stream function anomalies within the subtropical cells in both hemispheres (Figs. 8a, b). However, a more prominent response is the clockwise MOC anomaly near the lower boundary of the southern subtropical cell that is centered between the warm and cold cells (Figs. 8a, d). This anomalous circulation occupies a large fraction of the upper ocean in the southern hemisphere and extends to the northern hemisphere, bounded approximately by the 5°C to 20°C isotherms (0–1000 m, Figs. 2b, c) and spanning a latitudinal range from 50°S to 10°N, with the maximum change exceeding 2.5 Sv (1 Sv = 10^6 m^3 s^{-1}). This circulation anom-

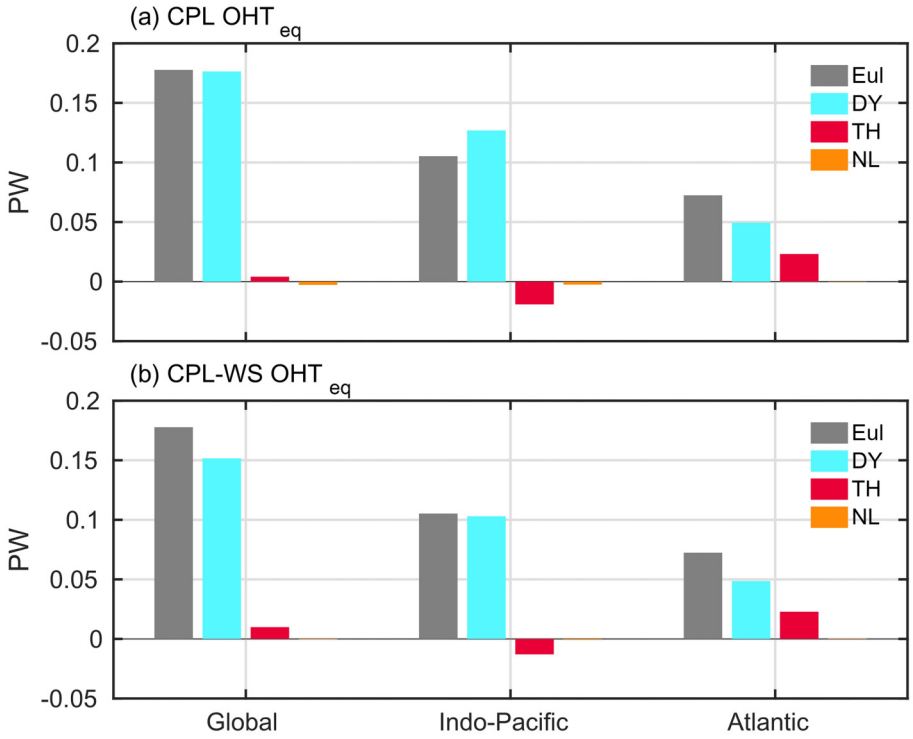

Fig. 7. The cross-equatorial Eulerian mean OHT response (PW) in (a) CPL and (b) CPL-WS. The Eulerian mean OHT (gray) is decomposed into dynamic (blue), thermodynamic (red), and nonlinear (orange) components. The cross-equatorial OHT is calculated as the OHT average between 10°S–10°N.

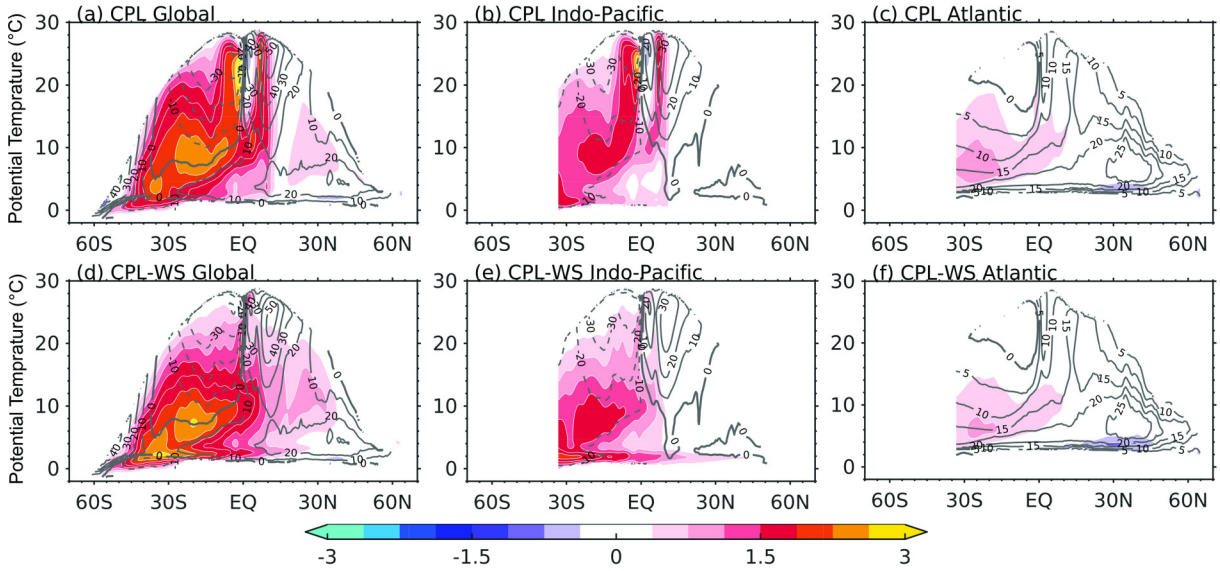

Fig. 8. The Eulerian-mean MOC response (Sv) in (upper panel) CPL and (lower panel) CPL-WS in the temperature-latitude coordinate for (a, d) the global ocean, (b, e) the Indo-Pacific ocean, and (c, f) the Atlantic. Superimposed is the corresponding mean MOC in CTRL-CPL. Positive (negative) values indicate a clockwise (counter-clockwise) circulation.

aly can produce a strong northward OHT anomaly owing to the large temperature difference between its upper and lower branches. The intrusion of the MOC anomalies into the northern hemisphere also plays a key role in spreading the warming signal to the northern hemisphere (Fig. 9). Although the clockwise MOC anomaly appears in both the Indo-Pacific and Atlantic basins (Figs. 8b, c), its magnitude is much larger in the former, which explains why the cross-equatorial dynamic OHT response is more significant there (Fig. 7a). Superimposing the anomalous MOC response to the background MOC, we can see that the deep circulation is weakened overall and the center of gravity of the cell becomes shallower (Fig. 8d). This feature is to be expected in response to a surface buoyancy source.

Note both the heat flux perturbation and the related sea ice melting(Figs. 4g, h) can serve as surface buoyancy sources and thus contribute to the thermohaline circulation changes. To quantitatively separate the respective contributions from the heat flux and the freshwater flux, we computed the buoyancy flux Q_B at the ocean surface as follows:

$$Q_B = \alpha \frac{\mathrm{SHF}}{\rho c_p} + \beta S_0 \mathrm{FWF} = Q_T + Q_S \,, \tag{6}$$

where SHF is the net surface heat flux, FWF is the net freshwater flux into the surface, ρ and c_p are the density and heat capacity of seawater, $\alpha = 1.67 \times 10^{-4}$ °C^{-1} and $\beta = 0.78 \times 10^{-3}$ psu^{-1} are the thermal and haline coefficients of expansion, S_0 is the reference surface salinity. Positive Q_B denotes an influx into the sea surface so that the surface layer becomes more buoyant. Expressed as Eq. (6) above, Q_B can be decomposed into contributions from the surface heat flux (Q_T) and the freshwater flux (Q_S), their responses in CPL are presented in Fig. 10. It can be seen that the surface heat flux component Q_T largely dominates Q_B in most of the Southern Ocean, corresponding to the strong temperature changes which occur there (Fig. 9). An exception is the region south of 65°S where sea ice melting occurs, the freshwater flux component Q_S overwhelms Q_T which results in a local freshening maxima in the vicinity of this location.

When the surface wind stress is prescribed and the ocean circulation is solely driven by the buoyancy flux, the clockwise MOC anomaly in the subtropical cells largely disappeared (cf. Figs. 8b, d), resulting in only ~20% reduction in the dynamical OHT across the equator (Fig. 7b). This much smaller contribution from the wind-driven response can be explained by the very weak cross-equatorial component of flow in the wind-induced subtropical cell response (Figs 8a, b), in contrast to what is depicted in Green and Marshall (2017; see their Fig. 6). Therefore, the MOC anomaly due to the thermal effect of the warming plays a much more important role in both ocean basins.

As shown in Fig. 7, the advection of temperature anomaly by the mean circulation also contributes to the cross-equatorial OHT response. Figure 9 shows the zonal mean temperature anomalies overlaid on top of the background mean MOC. The positive contribution to OHT from the thermodynamic component in the Atlantic (Fig. 7a) can be readily attributed to the ocean temperature change. The warming in the Atlantic is mainly confined in the upper branch of the Atlantic MOC that is directed northward throughout the basin, giving rise to a net northward ocean heat transport. In the Indo-Pacific, the almost symmetric subtropical cells with respect to the equator only project weakly onto the cross-equatorial flow (in fact, weakly southward in the upper branch), thus the mean subtropical cell transports the anomalous warmth southward, contributing negatively to the total northward OHT response at the equator. Overall, similar thermodynamic contributions still hold in the CPL-WS experiments, because the response of the wind-driven circula-

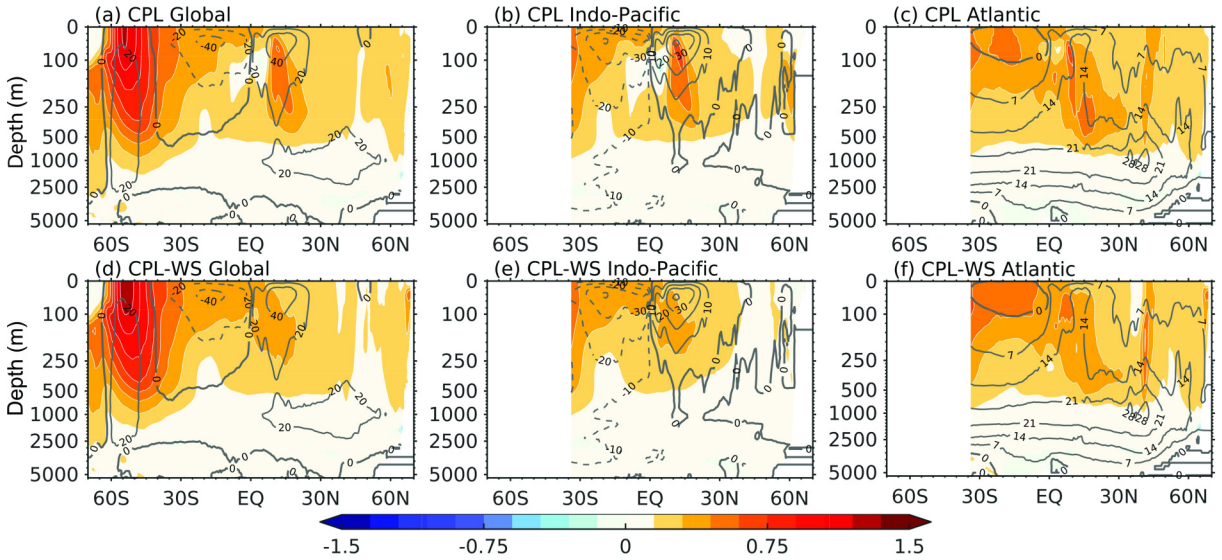

Fig. 9. The zonal mean potential temperature response (°C, shading) in (upper panel) CPL and (lower panel) CPL-WS for (a, d) the global ocean, (b, e) the Indo-Pacific, and (c, f) the Atlantic. The contours superimposed indicate the corresponding mean MOC (Sv) in CTRL-CPL.

tion is of secondary importance to begin with regarding the redistribution of heat in the global oceans (comparing the lower panel to the upper panel in Fig. 9). The weak subsurface cooling in the tropics of the Indo-Pacific Ocean is a result of thermocline shoaling, which is in turn caused by the cyclonic wind stress curl anomaly there (e.g., Luo et al., 2015).

Since the wind stress overriding experiments already show that the robust MOC anomaly between warm and cold cells is not wind-driven (Fig. 8), it can therefore be understood by looking into the temperature and density responses. According to Fig. 11, the water density is reduced more in the Southern Ocean than in the tropics, inducing a tilting of the density surface. Conceptually, supposing the circulation anomaly is solely caused by changes in density (Figs. 11d, f), on the same pressure level, the anomalous lighter seawater in the Southern Ocean would be subjected to the same upward pressure gradient force as the anomalous heavier seawater near the tropics. Consequently, the lighter seawater tends to rise more rapidly than the heavier seawater, resulting in a clockwise circulation anomaly between the Southern Ocean and the tropics, which alternatively can be thought of as being driven by a negative solenoidal effect in the zonal direction.

5. Conclusion

The primary goal of this study is to investigate the role of active ocean dynamics in modulating the cross-equatorial AHT and ITCZ shift responses to an external thermal

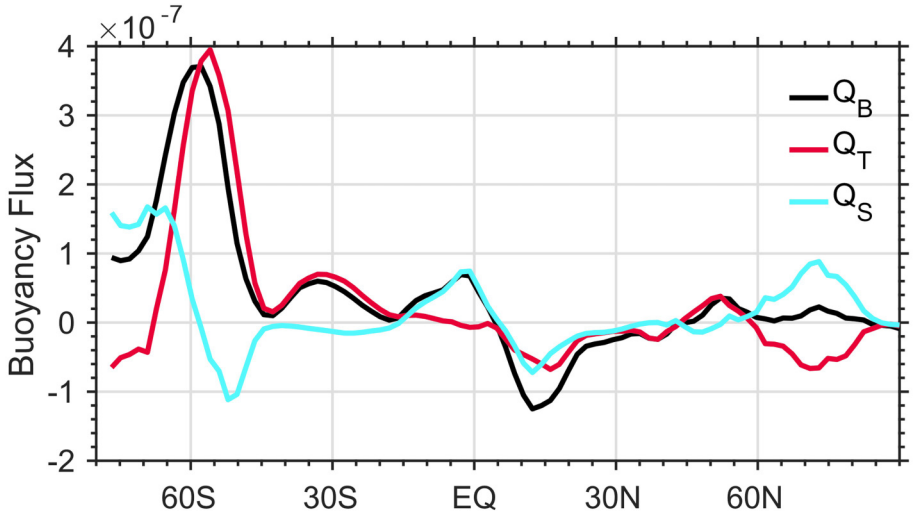

Fig. 10. The zonal mean changes of buoyancy flux Q_B (black; kg m^{-2} s^{-1}) and its surface heat flux component Q_t (red), and freshwater flux component Q_s (blue) in CPL.

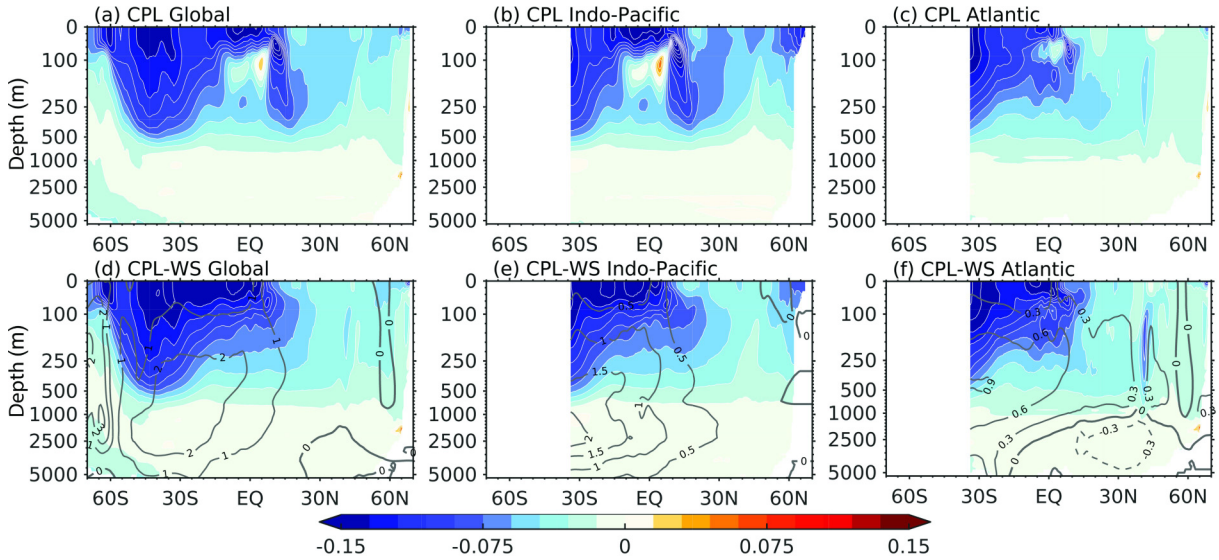

Fig. 11. The zonal mean potential density response (kg m^{-3}) in (upper panel) CPL and (lower panel) CPL-WS for (a, d) the global ocean, (b, e) the Indo-Pacific, and (c, f) the Atlantic. Superimposed in d–f are the corresponding Eulerian-mean MOC anomalies (Sv) in CPL-WS, solely driven by density changes (in the absence of wind stress changes).

forcing placed in the Southern Ocean. The main findings are as follows:

- Perturbing the Southern Ocean with an external thermal forcing leads to northward cross-equatorial energy transport and a southward ITCZ shift. However, the ITCZ shift in a slab ocean model is largely overestimated as the interhemispheric energy imbalance can only be restored by the atmosphere alone. When active ocean dynamics are included, most of the cross-equatorial energy transport takes place in the ocean, thus significantly alleviating the burden of the atmosphere in cross-equatorial energy transport and reducing the shift in ITCZ by a factor of 10. This demonstrates the profound importance of ocean dynamics upon the buffering of global energetics.
- Both the Indo-Pacific and the Atlantic can contribute to the northward cross-equatorial OHT mainly through changing its Eulerian-mean circulation (i.e., the dynamic component), while the changes in the thermodynamic component can explain about 30% of the cross-equatorial OHT response in the Atlantic.
- The major Eulerian-mean circulation change responsible for the dynamic OHT response is a clockwise anomalous overturning circulation below the southern hemisphere subtropical cell. The large temperature difference between its upper and lower branches makes it efficient in transporting energy northward and across the equator in both the Indo-Pacific and the Atlantic Oceans.
- The above circulation change is largely attributed to the thermohaline and is driven by the density anomalies. Therefore, shutting down the wind stress only exerts limited impacts on cross-equatorial OHT response.

The above results first verify the finding in recent studies (Kay et al., 2016; Hawcroft et al., 2017; Green and Marshall, 2017; Yu and Pritchard, 2019), i.e., the inclusion of a dynamical ocean would lead to the partitioning of the cross-equatorial energy transport response to external heating forcing in the Southern Ocean, and thereby largely reduce the ITCZ shift response compared to that in the climate system with a motionless slab ocean model. Most of the existing hypotheses for the ocean's buffering effect involve the mechanisms related to changes in subtropical cells (Held, 2001; Schneider et al., 2014; Kay et al., 2016; Green and Marshall, 2017) or in the AMOC (Frierson et al., 2013; Fučkar et al., 2013; Marshall et al., 2014; Yu and Pritchard, 2019). However, through a wind stress overriding experiment and a careful examination of the responses in OHT and ocean circulation, we find that the buffering effect of the ocean has resulted from a circulation anomaly that covers a broad range of the southern hemisphere ocean and extends to the northern hemisphere ocean. This circulation anomaly is largely thermohaline driven and can efficiently transport anomalous energy northward, which in turn reduces the response in the cross-equatorial AHT and the ITCZ shift.

It should be noted that, although the contribution from wind stress changes to the cross-equatorial OHT is relatively small in this study, it may vary according to the location of the forcing. The energy forcing here is placed in the Southern Ocean, where deep ocean convection prevails, and the surface thermal forcing can penetrate deeper and effectively alter the thermal and density structure of the interior ocean and thus induce an anomalous thermohaline circulation (Figs. 9 and 11). However, if the forcing were placed within the tropics or even the entire southern hemisphere, the changes in wind stress and the associated wind-driven subtropical cells may become larger and contribute more to the cross-equatorial OHT. We leave this issue for future investigation.

Acknowledgments. This work is supported by the National Key Research and Development Program of China (2018YFA0605702) and the National Natural Science Foundation of China (NSFC; 41906002, 91858210, 41976006, and 41776009). The model outputs generated and/or analyzed during the current study will be available to the public at (https://github.com/fliuouc/data_share), the data archiving is underway. For more details, please contact the corresponding author (fliu@ouc.edu.cn).

REFERENCES

Aagaard, K., and P. Greisman, 1975: Toward new mass and heat budgets for the Arctic Ocean. *J. Geophys. Res.*, **80**, 3821–3827, https://doi.org/10.1029/jc080i027p03821.

Broccoli, A. J., K. A. Dahl, and R. J. Stouffer, 2006: Response of the ITCZ to northern hemisphere cooling. *Geophys. Res. Lett.*, **33**, L01702, https://doi.org/10.1029/2005GL024546.

Chiang, J. C. H., and C. M. Bitz, 2005: Influence of high latitude ice cover on the marine Intertropical Convergence Zone. *Climate Dyn.*, **25**, 477–496, https://doi.org/10.1007/s00382-005-0040-5.

Czaja, A., and J. Marshall, 2006: The partitioning of poleward heat transport between the atmosphere and ocean. *J. Atmos. Sci.*, **63**, 1498–1511, https://doi.org/10.1175/JAS3695.1.

Dai, H., H. Yang, and J. Yin, 2017: Roles of energy conservation and climate feedback in Bjerknes compensation: a coupled modeling study. *Clim. Dyn.*, **49**, 1513–1529, https://doi.org/10.1007/s00382-016-3386-y.

Donohoe, A., J. Marshall, D. Ferreira, K. Armour, and D. Mcgee, 2014: The interannual variability of tropical precipitation and interhemispheric energy transport. *J. Clim.*, **27**, 3377–3392, https://doi.org/10.1175/JCLI-D-13-00499.1.

Farneti, R., and G. K. Vallis, 2013: Meridional energy transport in the coupled atmosphere-ocean system: Compensation and partitioning. *J. Climate*, **26**, 7151–7166, https://doi.org/10.1175/JCLI-D-12-00133.1.

Fox-Kemper, B., R. Ferrari, and R. Hallberg, 2011: Parameterization of mixed layer eddies. Part I: Theory and diagnosis. *J. Phys. Oceanogr*, **39**, 61–78, https://doi.org/10.1175/2007jpo3792.1.

Frierson, D. M. W., and Coauthors, 2013: Contribution of ocean overturning circulation to tropical rainfall peak in the northern hemisphere. *Nature Geoscience*, **6**, 940–944,

https://doi.org/10.1038/ngeo1987.

Fučkar, N. S., S. P. Xie, R. Farneti, E. A. Maroon, and D. M. W. Frierson, 2013: Influence of the extratropical ocean circulation on the intertropical convergence zone in an idealized coupled general circulation model. *J. Climate*, **26**, 4612–4629, https://doi.org/10.1175/JCLI-D-12-00294.1.

Gent, P. R., and J. C. Mcwilliams, 1990: Isopycnal mixing in ocean circulation models. *J. Phys. Oceanogr.*, **20**, 150–155, https://doi.org/10.1175/1520-0485(1990)020<0150:IMIOCM>2.0.CO;2.

Green, B., and J. Marshall, 2017: Coupling of trade winds with ocean circulation damps ITCZ shifts. *J. Climate*, **30**, 4395–4411, https://doi.org/10.1175/JCLI-D-16-0818.1.

Held, I. M., 2001: The partitioning of the poleward energy transport between the tropical ocean and atmosphere. *J. Atmos. Sci.*, **58**, 943–948, https://doi.org/10.1175/1520-0469(2001)058<0943:tpotpe>2.0.co;2.

Hawcroft, M., J. M. Haywood, M. Collins, A. Jones, A. C. Jones, and G. Stephens, 2017: Southern Ocean albedo, inter-hemispheric energy transports and the double ITCZ: Global impacts of biases in a coupled model. *Climate Dyn.*, **48**, 2279–2295, https://doi.org/10.1007/s00382-016-3205-5.

He, C. F., Z. Y. Liu, and A. X. Hu, 2019: The transient response of atmospheric and oceanic heat transports to anthropogenic warming. *Nature Climate Change*, **9**, 222–226, https://doi.org/10.1038/s41558-018-0387-3.

Hwang, Y. T., S. P. Xie, C. Deser, and S. M. Kang, 2017: Connecting tropical climate change with Southern Ocean heat uptake. *Geophys. Res. Lett.*, **44**, 9449–9457, https://doi.org/10.1002/2017GL074972.

Hwang, Y.-T., and D. M. W. Frierson, 2013: Link between the double-Intertropical Convergence Zone problem and cloud biases over the Southern Ocean. *Proc. Natl. Acad. Sci.*, **110**, 4935–4940, https://doi.org/10.1073/pnas.1213302110.

Jayne, S. R., and J. Marotzke, 2002: The oceanic eddy heat transport *J.Phys.Oceanogr.*,**32**,3328–3345,https://doi.org/10.1175/1520-0485(2002)032<3328:toeht>2.0.co;2.

Kay, J. E., C. Wall, V. Yettella, B. Medeiros, C. Hannay, P. Caldwell, and C. Bitz, 2016: No access global climate impacts of fixing the Southern Ocean shortwave radiation bias in the Community Earth System Model (CESM). *J. Clim.*, **29**, 4617–4636, https://doi.org/10.1175/JCLI-D-15-0358.1.

Kang, S. M., I. M. Held, D. M. W. Frierson, and M. Zhao, 2008: The response of the ITCZ to extratropical thermal forcing: Idealized slab-ocean experiments with a GCM. *J. Climate*, **21**, 3521–3532, https://doi.org/10.1175/2007JCLI2146.1.

Kang, S. M., Y. Shin, and S.-P. Xie, 2018: Extratropical forcing and tropical rainfall distribution: energetics framework and ocean Ekman advection. *Npj Climate and Atmospheric Science*, **1**, 20172, https://doi.org/10.1038/s41612-017-0004-6.

Klinger, B. A., and J. Marotzke, 2000: Meridional heat transport by the subtropical cell. *J. Phys. Oceanogr.*, **30**, 696–705, https://doi.org/10.1175/1520-0485(2000)030<0696:MHTBTS>2.0.CO;2.

Lembo, V., V. Lucarini, and F. Ragone, 2020: Beyond forcing scenarios: Predicting climate change through response operators in a coupled general circulation model. *Scientific Reports*, **10**, 8668, https://doi.org/10.1038/s41598-020-65297-2.

Liu, F. K., Y. Y. Luo, J. Lu, and X. Q. Wan, 2017a: : Response of the tropical Pacific Ocean to El Niño versus global warming. *Climate Dyn.*, **48**, 935–956, https://doi.org/10.1007/s00382-016-3119-2.

Liu, F. K., Y. Y. Luo, J. Lu, O. Garuba, and X. Q. Wan, 2017b: Asymmetric response of the equatorial Pacific SST to climate warming and cooling. *J. Climate*, **30**, 7255–7270, https://doi.org/10.1175/JCLI-D-17-0011.1.

Liu, W., J. Lu, S. P. Xie, and A. Fedorov, 2018b: : Southern Ocean Heat Uptake, redistribution, and storage in a warming climate: The role of meridional overturning circulation. *J. Climate*, **31**, 4727–4743, https://doi.org/10.1175/JCLI-D-17-0761.1.

Long, S.-M., S.-P. Xie, X.-T. Zheng, and Q. Y. Liu, 2014: Fast and slow responses to global warming: Sea surface temperature and precipitation patterns. *J. Climate*, **27**, 285–299, https://doi.org/10.1175/JCLI-D-13-00297.1.

Lu, J., and B. Zhao, 2012: The role of oceanic feedback in the climate response to doubling CO_2. *J. Climate*, **25**, 7544–7563, https://doi.org/10.1175/JCLI-D-11-00712.1.

Luo, Y. Y., J. Lu, F. K. Liu, and W. Liu, 2015: Understanding the El Niño-like oceanic response in the tropical Pacific to global warming. *Climate Dyn.*, **45**, 1945–1964, https://doi.org/10.1007/s00382-014-2448-2.

Marshall, J., A. Donohoe, D. Ferreira, and D. McGee, 2014: The ocean's role in setting the mean position of the Inter-Tropical Convergence Zone. *Climate Dyn.*, **42**, 1967–1979, https://doi.org/10.1007/s00382-013-1767-z.

Schneider, T., T. Bischoff, and G. H. Haug, 2014: Migrations and dynamics of the intertropical convergence zone. *Nature*, **513**, 45–53, https://doi.org/10.1038/nature13636.

Schneider, T., 2017: Feedback of atmosphere-ocean coupling on shifts of the intertropical convergence zone. *Geophys. Res. Lett.*, **44**, 11644–11653, https://doi.org/10.1002/2017GL075817.

Stouffer, R. J., 2004: Time scales of climate response. *J. Climate*, **17**, 209–217, https://doi.org/10.1175/1520-0442(2004)017<0209:TSOCR>2.0.CO;2.

Treguier, A. M., M. H. England, S. R. Rintoul, G. Madec, J. Le Sommer, and J. M. Molines, 2007: Southern Ocean overturning across streamlines in an eddying simulation of the Antarctic Circumpolar Current. *Ocean Science*, **3**, 491–507, https://doi.org/10.5194/os-3-491-2007.

Trenberth, K. E., and J. M. Caron, 2001: Estimates of meridional atmosphere and ocean heat transports. *J. Climate*, **14**, 3433–3443, https://doi.org/10.1175/1520-0442(2001)014<3433:EOMAAO>2.0.CO;2.

Yang, H. J., Q. Li, K. Wang, Y. Sun, and D. X. Sun, 2015: Decomposing the meridional heat transport in the climate system. *Climate Dyn.*, **44**, 2751–2768, https://doi.org/10.1007/s00382-014-2380-5.

Yang, H. J., and H. J. Dai, 2015: Effect of wind forcing on the meridional heat transport in a coupled climate model: Equilibrium response. *Climate Dyn.*, **45**, 1451–1470, https://doi.org/10.1007/s00382-014-2393-0.

Yu, S., and M. S. Pritchard, 2019: A strong role for the AMOC in partitioning global energy transport and shifting ITCZ position in response to latitudinally discrete solar forcing in CESM1.2. *J. Climate*, **32**, 2207–2226, https://doi.org/10.1175/JCLI-D-18-0360.1.